Global Environmental Science
www.sciltp.com/journals/ges

Article

Hierarchical Sandwich-Type Hetero-Wetting Nanofibrous Membrane toward Nano-Scaled Oil/Water Emulsion Separation

Linlin Yan [1,2], Mengmeng Zhang [1], Chen Chen [1], Mi Zhou [1], Kai Wang [1,2], Yuhua Gao [3], Pengcheng Liu [2], Dalong Li [1] and Xiquan Cheng [1,2,*]

[1] State Key Laboratory of Urban-rural Water Resource and Environment, School of Marine Science and Technology, Harbin Institute of Technology, Weihai 264209, China
[2] Weihai Key Laboratory of Water Treatment and Membrane Technology, Shandong Sino-European Membrane Technology Research Institute Co., Ltd., Weihai 264209, China
[3] Institute of Energy Resources, Hebei Academy of Sciences, Shijiazhuang 050081, China
* Correspondence: chengxiquan@hit.edu.cn

How To Cite: Yan, L.; Zhang, M.; Chen, C.; et al. Hierarchical Sandwich-Type Hetero-Wetting Nanofibrous Membrane toward Nano-Scaled Oil/Water Emulsion Separation. *Glob. Environ. Sci.* **2026**, *2*(1), 53–66. https://doi.org/10.53941/ges.2026.100005

Publication History

Received: 10 October 2025
Revised: 30 November 2025
Accepted: 23 December 2025
Published: 14 January 2026

Keywords

hetero-wetting membranes; electrospinning nanofiber; sieving-repulsion-adsorption mechanism; nano-scaled oil/water emulsions separation

Highlights

- The hetero-wetting nanofibrous membrane with sandwich structure was fabricated
- A novel "sieving-repulsion-adsorption" separation mechanism was proposed
- The membrane can efficiently remove oil droplets sub-150 nm (TOC less than 3 ppm)
- The membrane has superior cycle stability for oil/water emulsion separation

Abstract: The ever-increasing discharge of oily sewage poses serious threats to marine ecosystem and human health, which has become a severe environmental problem globally. With high porosity, interconnected porous architectures and tunable surface wettability, superwetting nanofiber membranes have been proven effective in remediating oily sewage. However, constrained by their micron-scale pores, nanofiber membranes demonstrate insufficient separation efficiency for sub-150 nm emulsified oil droplets, making it difficult to meet the standards of regulations for discharging oily sewage in various countries and regions. Herein, a "sieving-repulsion-adsorption" mechanism was proposed to break the limitation of "trade-off" between permeability and selectivity via the designed hetero-wetting nanofiber membrane, which was engineered by intercalating discrete hydrophobic polydimethylsiloxane (PDMS) microdomains between hydrophilic polyethylene oxide (PEO)-based hydrogels modified polyacrylonitrile (PAN) nanofiber membranes. The hetero-wetting architecture improves water transport under the synergistic effect of hydrophobic/hydrophilic layers while captures the tiny oil droplets via hydrophobic/oleophilic PDMS microdomains, thereby achieving high emulsion permeance of 22,308 $L \cdot m^{-2} \cdot h^{-1} \cdot bar^{-1}$ with high separation efficiency of 99.97% and total organic carbon (TOC) content less than 3 ppm. Notably, the membrane demonstrates exceptional fouling resistance (94.6% permeance recovery) and cyclic stability, outperforming most previously reported state-of-the-art nanofiber membranes. This sandwich-type hetero-wetting nanofibrous membrane provides new insights into advanced membranes fabrication for low-carbon and efficient treatment of nano-scaled oil-in-water emulsions.

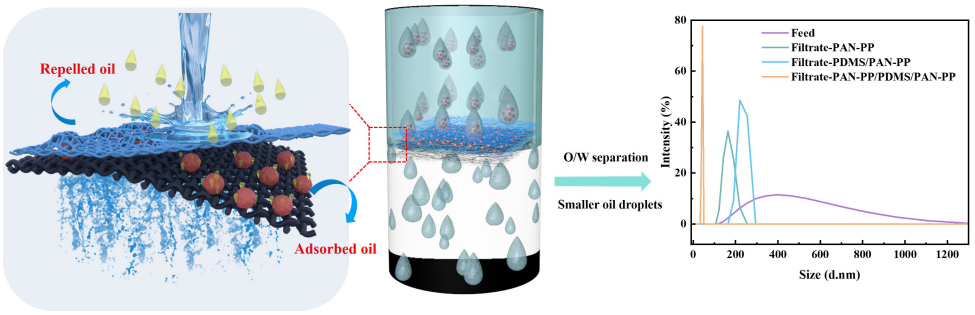

1. Introduction

The discharge of poorly degradable oily wastewater originating from domestic, industrial and accidental petroleum release sources disrupts environmental systems, kills aquatic creatures, and poses significant risks to public health [1–4]. Depending on the dispersed phase, these emulsions can be broadly classified into dispersed oil, suspended oil, emulsified oil, and dissolved oil. Compared with insoluble mixtures, oil-in-water emulsions, stabilized by surfactants and ranging in size from tens of nanometers to several microns, represent challenging separation targets among environmentally hazardous wastewater types [5–7]. In particular, nano-scaled oil-in-water emulsions are relatively hard to separate due to small size and good stability [8]. Compared with traditional emulsion separation technologies like gravity sedimentation [9], air flotation [10] and centrifugal separation [11], superwetting nanofiber membranes have emerged as promising candidates for emulsion separation owing to their interconnected porous architectures, tunable surface wettability, and enhanced permeability [12,13]. In general, high-performance membranes are designed based on two key principles: (I) the pore size of the membrane should match the size of the emulsions; (II) the as-prepared membranes should exhibit special wettability. For instance, hydrophilic/oleophobic membranes allow water to penetrate while intercepting oil, thereby enabling effective separation of O/W emulsions. However, due to the unstable rheological characteristics of electrospinning fluid, it is difficult to fabricate nanofibers with an average diameter beneath 100 nm, resulting the pore size of the electro-spun nanofiber membrane at the micron-level. Therefore, the superwetting nanofiber membranes are insufficient to remove sub-150 nm oil droplets from emulsions due to their relatively large pores, which usually fails to meet the standard of the Oslo-Paris (OSPAR) convention (TOC less than 30 ppm) and regulations for discharging oily wastewater in China (TOC less than 10 ppm) [5,14–16]. It is still a challenge to construct nanofiber membranes for highly efficient water remediation of oil-in-water emulsions, especially for nano-scaled oil droplets in the emulsions [17–19].

Recently, several reports found that the asymmetric surface wettability of Janus membranes can significantly improve the separation efficiency of oil-in-water emulsions [20–22]. The wettability difference between the two sides of Janus membranes creates a surface energy gradient, which facilitates directional water penetration while blocking oil droplets [23]. For example, Qin et al. fabricated a Janus membrane by electrospinning polylactic acid (PLA)/carbon nanotubes (CNTs) and PLA/SiO_2 as the two sides of the nanofiber membrane. The prepared membrane exhibited a “water diode” effect, facilitating unidirectional liquid transport without external pressure and demonstrating excellent separation efficiency for oil-in-water emulsions, with 100% rejection of oil droplets larger than 50 nm [24]. However, the serious membrane fouling lead to irreversible performance degradation during the treatment of oil-in-water emulsions. This reduction is primarily attributed to the continuous hydrophobic layers of the Janus membranes, which may reduce water permeance and increase oil contamination [25,26].

In current work, to improve the Janus membrane’s anti-fouling performance and efficient separation of tiny oil droplets in oil-in-water emulsions, we fabricated hetero-wetting membranes with hydrophilic/hydrophobic/hydrophilic sandwich-type structures by integrating discrete hydrophobic/oleophilic PDMS microdomains into hydrophilic PEO hydrogel-modified PAN (PAN-PP) composite nanofiber layers through stepwise electrospinning/electrospraying of the PAN-PP supporting layer, PDMS intermediate layer and PAN-PP selective layer (Figure 1). Specifically, as shown in Figure 1a, a hydrophilic cross-linked PEO-based hydrogel network was formed via the epoxy ring-opening reaction between polyether amine (PEA) and polyethylene glycol diglycidyl ether (PEGDGE) during the PAN electrospinning process. Multi-hydrophilic groups (-CH_2-O-CH_2-, -OH, etc.) were successfully introduced onto the surface of the PAN membrane (PAN-PP membrane, supporting layer), which could improve the hydrophilicity of the membrane surface for ultrafast water permeation. After incorporating PDMS microdomains, a hetero-wetting nanofiber membrane that creates a wettability gradient was formed to accelerate water penetration. The discrete hydrophobic/oleophilic PDMS microdomains could capture sub-150 nm oil droplets that pass through the selective layer, thereby improving separation efficiency. Simultaneously, the PEO-based hydrogels in the hydrophilic selective layer (PAN-PP) promote the formation of a hydration layer, reducing membrane fouling by oil droplets. The special sandwich structure combined the size sieving and repulsion mechanism of the hydrophilic selective layer and the adsorption mechanism of the hydrophobic layer, which is expected to break the limitations of traditional single superwetting membranes and Janus membranes. The surface wettability and emulsion separation performance of sandwich-type hetero-wetting membrane has been comprehensively investigated. This study provides a practical reference for the development of efficient nanofiber membranes applied to oil-in-water emulsion separation, demonstrating great potential application value in the sustainable utilization of water resources as well as the inhibition for toxicity of oil pollution on the microbial community.

 https://doi.org/10.53941/ges.2026.100005

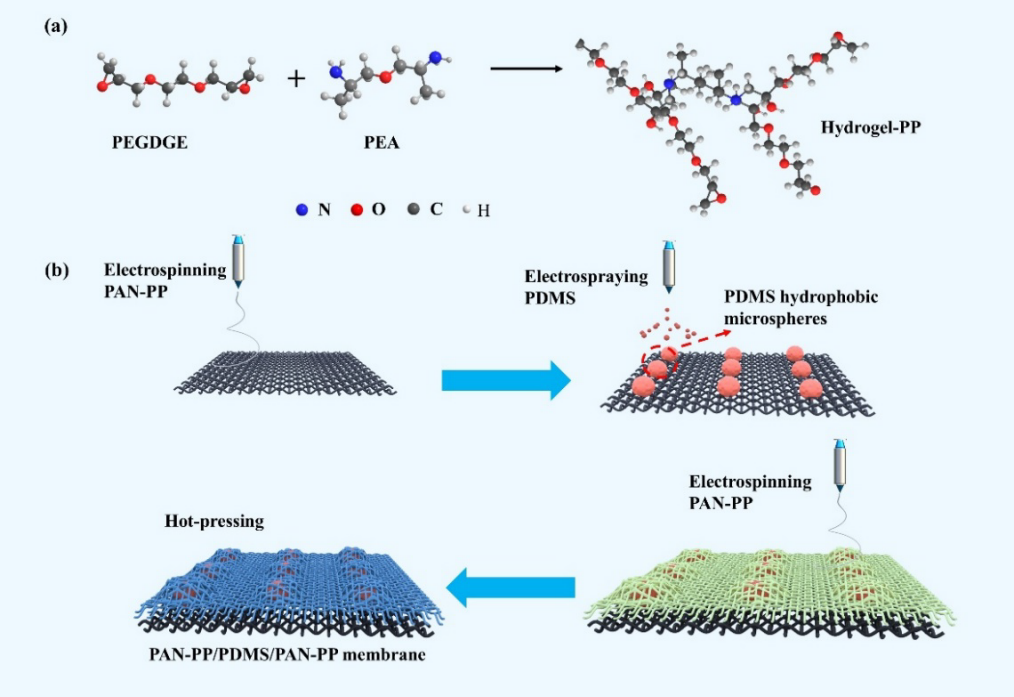

Figure 1. (**a**) Formation mechanism of PEO hydrogels; (**b**) Schematic diagram of the formation of the hetero-wetting PAN-PP/PDMS/PAN-PP nanofiber membrane.

2. Materials and Methods

2.1. Materials

Polyacrylonitrile (PAN, M. W. = 150,000) was acquired from Huachuang Plasticizing Co., Ltd. (Suzhou, China). Polyetheramine (PEA D-400) was purchased from Macklin Biochemical Co., Ltd. (Shanghai, China). Sodium chloride (analytical grade), N, N-Dimethylformamide (DMF) and tetrahydrofuran (THF) were obtained from Chemical Industry Co., Ltd. (Tianjin, China). Polyoxyethylene bis (glycidyl ether) (PEGDGE), trichloromethane ($CHCl_3$), sodium dodecyl sulfate (SDS), n-hexane, toluene, dichloromethane, xylene, n-octane, hexadecane, oil red O (Sudan III), hydrochloric acid (HCl, 37%) and sodium hydroxide (analytical purity) were all acquired from Aladdin Chemistry Co., Ltd. (Shanghai, China). Polydimethylsiloxane (PDMS) and its curing agent were purchased from Dow Corning Co., Ltd. (Shanghai, China). 4A molecular sieve was obtained from Kelong Chemical Reagent Co., Ltd. (Chengdu, China). Ethanol was sourced from Shuangshuang Chemical Co., Ltd. (Yantai, China). Ultrapure water was used for preparing various solutions. Unless otherwise stated, all chemicals were used directly as obtained without further purification.

2.2. Fabrication of Hetero-Wetting Nanofiber Membranes

Different nanofiber membranes were prepared by electrospinning-spray technique. The hetero-wetting membranes (PAN-PP/PDMS/PAN-PP) consisting of two hydrophilic layers and a middle hydrophobic layer were fabricated via an alternative stepwise electrospinning-spray technology combined with in-situ hydrophilic modification strategy and a heat treatment process. The PAN-PP precursor solution was formulated as follows: 15% PAN powder and 1.6% PEGDGE solution were dissolved in 82.6% DMF and stirred at 80 °C for 4 h. Then cooled to room temperature, after which 0.8% PEA was added and mixed for an additional 8 h. The PDMS precursor solution was made as follows: 8% PDMS solution was prepared by dissolving PDMS in THF and stirring the mixture at 30 °C for 12 h. Subsequently, the PAN-PP and PDMS solutions were poured into plastic syringes equipped with metal needles (inner diameters of 0.86 mm and 0.4 mm, respectively) and connected to the pumps of the electrospinning machine. The PAN-PP/PDMS/PAN-PP sandwich nanofiber membrane was fabricated by adjusting the conditions of the electrospinning-spray process. The syringes were alternately electrospun-sprayed onto the grounded rotating metal roller covered with aluminum foil. The negative voltage for both electrospinning and spray was maintained at 2 kV, while the positive voltages were set to 15 kV and 17 kV, respectively. The distances between the spinneret and the receiver were set to 15 cm for electrospinning and 8 cm for spraying, respectively. The PAN-PP solution was supplied at a rate of 0.6 $mL{\cdot}h^{-1}$, while the PDMS solution was delivered at 0.24 $mL{\cdot}h^{-1}$. The rotating metal drum receiver operated at a speed of 228 revolutions per minute (rpm). The electrospinning time for the PAN-PP support layer was 6 h, while the electrospinning time for the PAN-PP selective layer was 2.5 h. The electrospray time for the PDMS intermediate layer was 30 min (denoted as the PAN-PP/PDMS/PAN-PP membrane). The relative humidity was maintained at 35 ± 5% and the ambient temperature was set at 25 ± 5 °C.

After electrospinning, the precursor membranes were carefully removed from the collector and hot-pressed at 80 °C for 1 h. The preparation conditions, the concentration of PDMS were optimized. It was found that the separation performance for oil-in-water emulsions was optimal when the PDMS concentration was 8% (see Figure S1 for details). PAN-PP nanofiber membranes and PDMS/PAN-PP nanofiber membranes were prepared as control samples. For the PAN-PP nanofiber membranes, the electrospinning time was 8.5 h. As for the PDMS/PAN-PP membrane, it lacked the PAN-PP hydrophilic selective layer.

2.3. Characterization

The as-prepared membranes were analyzed using field-emission scanning electron microscopy (FESEM, Merlin Compact, Zeiss, Oberkochen, Germany) to examine their micromorphology and generate energy-dispersive X-ray spectroscopy (EDS) maps. Additionally, the surface roughness of the membranes was evaluated using laser confocal microscopy (CLSM, LSM700, Zeiss, Oberkochen, Germany). The phase distribution on the membrane surface was characterized by a laser microconfocal Raman spectrometer (Xplora Plus, HORIBA FRANCE SAS, Villeneuve-d'Ascq, France). The chemical structures of the newly fabricated membranes were analyzed via X-ray photoelectron spectroscopy (XPS; PHI5000, VersaProbe, Physical Electronics (Chanhassen, MN, USA)) and an ATR-FTIR spectrometer (TENSOR II, Bruker, Billerica, MA, USA). The porous characteristics of the membranes were measured by utilizing a bubble pressure filter membrane pore size analyzer (BSD-PB, Beijing BEST Instruments Company, Beijing, China). Differential scanning calorimetry (DSC) was employed to record the thermograms of the membranes recorded on a Mettler Toledo 821 e instrument (Bruker DSC 3100SA, Mettler Toledo, Columbus, OH, USA) over a temperature range of −70 °C to 100 °C. The total organic carbon (TOC) content of the feed and permeate solutions was measured by TOC analysis (Shimadzu TOC-LCPH, Kyoto, Japan). Water contact angles (WCA) and underwater oil contact angles (UOCA) were measured using a contact angle instrument (SL200KS, Kino Industry Co., Ltd., Boston, MA, USA). For contact angle measurements, the average value of five or more measurements was computed. Optical microscopy images of both the initial emulsion and the filtrate were captured using an optical digital microscope (DSX 510, Olympus, Tokyo, Japan). The size distribution of oil droplets in the emulsion and permeate was analyzed using a Malvern nanometer particle size and zeta potentiometer (Zetasizer Nano ZS90, Malvern Panalytical, Malvern, UK). To ensure the accuracy and representativeness of the data, each measurement was measured at least three times. The membrane was immersed in acids, bases, salts, and hot water for 5 days to examine its wetting stability. Besides, the membrane was directly placed in different pH solutions to investigate the wettability underwater.

2.4. Oil-in-Water Emulsions Separation Performance

The process of preparing surfactant-stabilized oil-in-water emulsions involves several key steps. First, oils stained with oil red O (50 mg·L^{-1}) were mixed into deionized water at a volume ratio of 1:99, with 100 mg·L^{-1} SDS added as a surfactant. The mixtures were then vigorously stirred for 8 h at 1000 rpm to obtain a homogeneous emulsion. An emulsion separation experiment was conducted by employing a dead-end filtration apparatus. The system maintained a constant liquid height of 10 cm with an effective filtration area of 1.77 cm^2. The permeance was calculated by measuring the volume of filtered liquid collected over 5 min using the following equation [27]:

$$L = \frac{V}{A \times t \times P} \quad (1)$$

where L (L·m^{-2}·h^{-1}·bar^{-1}) is the permeance of emulsion, V (L) is the volume of emulsion that permeates through the membrane, A (m^2) is the effective separation area, t (h) is the effective filtration time and P (bar) refers to the trans-membrane pressure. The TOC content of the feed and the filtrate after membrane filtration were measured, and the separation efficiency was acquired according to the following equation [28]:

$$R(\%) = （1 - \frac{TOC_p}{TOC_f}) \times 100\% \quad (2)$$

where TOC_p and TOC_f represent the total organic carbon concentrations (ppm) in the filtrate and feed emulsion, respectively.

To evaluate the anti-fouling performance of the prepared membranes for emulsion separation, the membranes were also tested for 20 times of measuring-washing cycles of emulsion separation, with each cycle tested for 5 min. After each separation test, the membranes were cleaned with water and the separation process was repeated to record the permeance and separation efficiency of each cycle. During the 60-min separation cycle, the membrane surface was rinsed with deionized water every 20 min. The irreversible fouling rate IRF (%) and permeance recovery rate PRR (%) of the prepared membranes were calculated using the following equations [29]:

$$IRF\ (\%) = 1 - \frac{L_{iw} - L_s}{L_0 - L_s} \times 100\% \quad (3)$$

$$PRR\ (\%) = \frac{L_{iw}}{L_0} \times 100\% \quad (4)$$

where L_{iw} (L·m^{-2}·h^{-1}·bar^{-1}) is the permeance after cleaning, L_s (L·m^{-1}·h^{-1}·bar^{-1}) is the emulsion permeance after scaling and L_0 (L·m^{-2}·h^{-1}·bar^{-1}) is the initial emulsion permeance.

 https://doi.org/10.53941/ges.2026.100005

3. Results and Discussions

3.1. Characterization of Hetero-Wetting PAN-PP/PDMS/PAN-PP Membrane

The chemical composition of the as-prepared membranes was tested by FT-IR (Figure 2a). The PAN-PP membrane exhibited a typical characteristic peak at 2242 cm^{-1}, which correspond to the stretching vibration of -CN group [30]. Additionally, a peak at 1100 cm^{-1} indicated the stretching vibration of the CH_2-O-CH_2 group, suggesting a cross-linking reaction between PEA and PEGDGE (Figure S2) [31]. Compared to the PAN-PP membrane, the PDMS/PAN-PP membrane exhibited peaks corresponding to Si-O-Si bond stretching at 1020 cm^{-1} and Si-CH_3 rocking vibrations at 801 cm^{-1} and 1260 cm^{-1}, respectively, confirming the presence of PDMS microdomains on the PAN-PP membrane surface [32]. All of these peaks also appeared in the FI-IR spectra of the PAN-PP/PDMS/PAN-PP membrane. In the XPS spectra of the PAN-PP membranes, only C, N and O elements were observed, while two new peaks at 154.1 eV (Si 2s) and 102.3 eV (Si 2p) appeared in the XPS spectra of the PDMS/PAN-PP and PAN-PP/PDMS/PAN-PP nanofiber membranes, indicating the existence PDMS microdomains (Figure 2b) [33]. As shown in Figure 2c, the C 1s spectra further showed that the presence of peaks at 285.9 eV (C-N) and 286.6 eV (C-O) in the PAN-PP membrane confirmed the successful incorporation of the PEA/PEGDGE cross-linked structure on the membrane surface [32]. In addition, three distinct peaks were identified at binding energies of 101.4 eV (Si-O), 102.4 eV (Si-O-Si) and 103.8 eV (Si-OH) in the fine Si spectra of the PDMS/PAN-PP membranes (Figure 2d), indicating the successful introduction of PDMS microdomains between the PAN-PP layers [34].

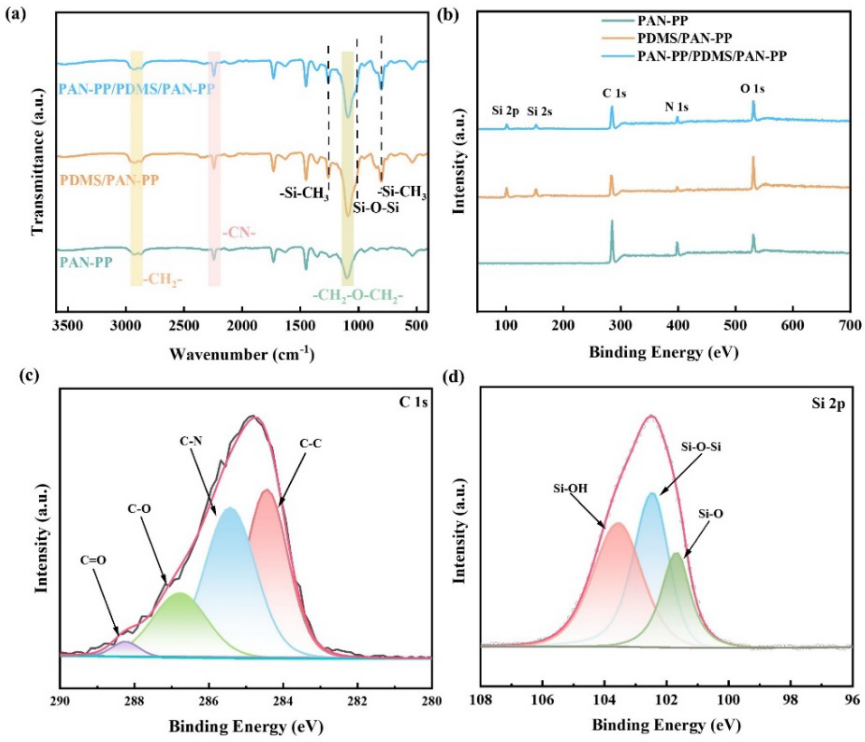

Figure 2. (**a**) FT-IR spectra and (**b**) XPS total spectra of PAN-PP, PDMS/PAN-PP and PAN-PP/PDMS/PAN-PP membranes; (**c**) C 1s XPS spectra of the PAN-PP membrane; (**d**) Si 2p XPS spectra of the PDMS/PAN-PP membrane.

The PAN-PP membrane exhibited a porous structure formed by stacked smooth and disordered nanofibers (Figure 3a), whereas micrometer-sized microdomains (3–6 μm in diameter) were randomly dispersed on the surface of the PDMS/PAN-PP membrane (Figure 3b). After the THF evaporates during the electro-spraying process, the PDMS precursor molecular chains will deposit on the fiber surface, re-aggregate, entangle, and eventually be solidified through heating and anchored onto the surface of the PAN-PP nanofibers, making it difficult to detach from the membrane. Interestingly, the microdomains disappeared and the morphology of the nanofiber membranes became smooth again after the deposition of the selection layer (Figure 3c). In addition, with increment of concentration of PDMS precursor, the diameter of PDMS microdomains became larger (Figure S3), while the surface of the PAN-PP/PDMS/PAN-PP nanofiber membranes remained smooth (Figure S4), indicating that the PDMS microdomains were fully covered by the PAN-PP selective layer. Cross-sectional SEM images of the PDMS/PAN-PP membrane showed that PDMS microdomains were dispersed on the surface of the PAN-PP (Figure S5). Meanwhile, cross-sectional SEM images of the 87 μm thick PAN-PP/PDMS/PAN-PP membrane

(Figure S6a) with a thickness of approximately 29 μm selective layer. Notably, the PDMS hydrophobic microdomains could not be observed since the PDMS microdomains were successfully covered by the selective layer (Figure S6b). The PAN-PP membrane demonstrated uniform surface distribution of C, N, and O elements (Figure S7a), confirming effective integration between the hydrogel and PAN nanofibers. As a comparison, the PDMS/PAN-PP membrane exhibited characteristic signals of C, N, O, and Si (Figure 3d). The Si distribution demonstrated PDMS attachment to nanofibers or in the formation of microspheres. Notably, C, N, O, and Si elements were also simultaneously detected of on the PAN-PP/PDMS/PAN-PP membrane surface (Figure S7b). The surface roughness of the prepared membranes was further examined (Figure 3e–g). After incorporating the discretely hydrophilic PDMS microdomains, the surface roughness (Ra) increased from 1.53 μm to 5.98 μm. After PAN-PP selective layer deposition, the surface roughness decreased to 3.32 μm. 2D Raman imaging (Figure S8a) of the as-prepared membranes validated PDMS micro-domains (red) discretely distributed on the PAN-PP supporting layer (blue), while Figure S8b,c mapped PEA/PEGDGE (red) within the tri-layer membrane. The lack of detectable PDMS signals in the PAN-PP/PDMS/PAN-PP membranes confirmed complete coverage by the PAN-PP selective layer [35].

The pore size of the PAN-PP nanofiber membrane was approximately 2.9 μm, decreasing to 2.7 μm after incorporating the PDMS hydrophobic microdomains (Figure 4a). Due to the coverage of the selective layer, the average pore size of the PAN-PP/PDMS/PAN-PP membrane was further reduced to 2.1 μm. Notably, the porosity of all nanofiber membranes exceeded 80% (Figure 4b). In addition, the DSC curves of the PAN-PP and PDMS/PAN-PP membranes showed that the enthalpy of melting decreased from 24.71 J·g^{-1} to 5.98 J·g^{-1} after the introduction of hydrophobic PDMS microdomains (Figure 4c), which was caused by the hydrophobicity of PDMS. After overlaying the PAN-PP selective layer, the enthalpy of melting increased to 43.41 J·g^{-1}, indicating the high hydration capacity. The adsorption capacity of the prepared membranes was further tested in Figure 4d. Similar to the results of DSC, the PAN-PP/PDMS/PAN-PP membrane exhibited the highest water adsorption capacity. As shown in Table S1, compared to the PAN-PP and PDMS/PAN-PP membranes, the non-refrigerated water content in the PAN-PP/PDMS/PAN-PP membrane increased to 82.85%, indicting its improved ability to bind water more effectively.

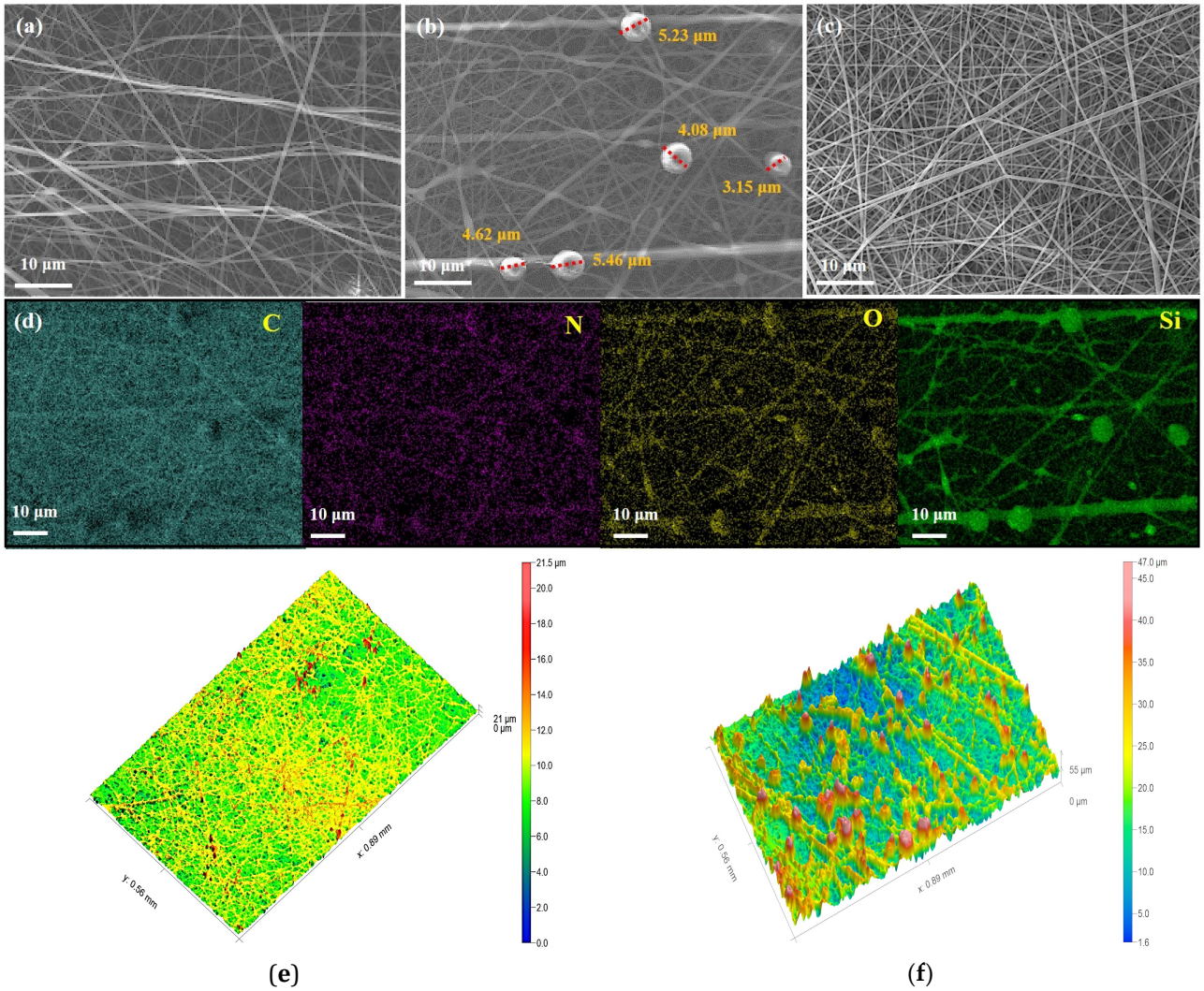

(e) (f)

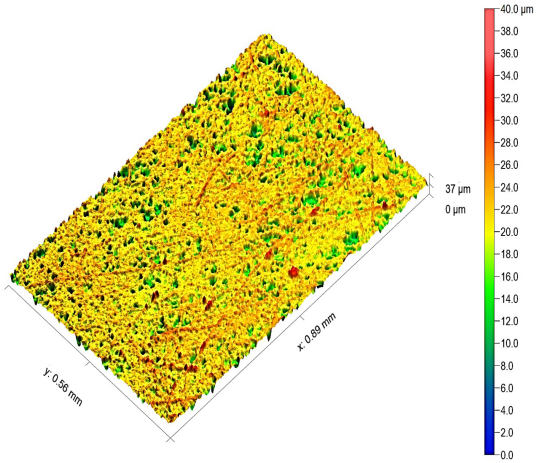

(g)

Figure 3. Morphologies of the prepared (**a**) PAN-PP; (**b**) PDMS/PAN-PP and (**c**) PAN-PP/PDMS/PAN-PP membranes; (**d**) EDS mapping images of the PDMS/PAN-PP membrane. Three-dimensional surface contour images of (**e**) PAN-PP; (**f**) PDMS/PAN-PP and (**g**) PAN-PP/PDMS/PAN-PP membranes.

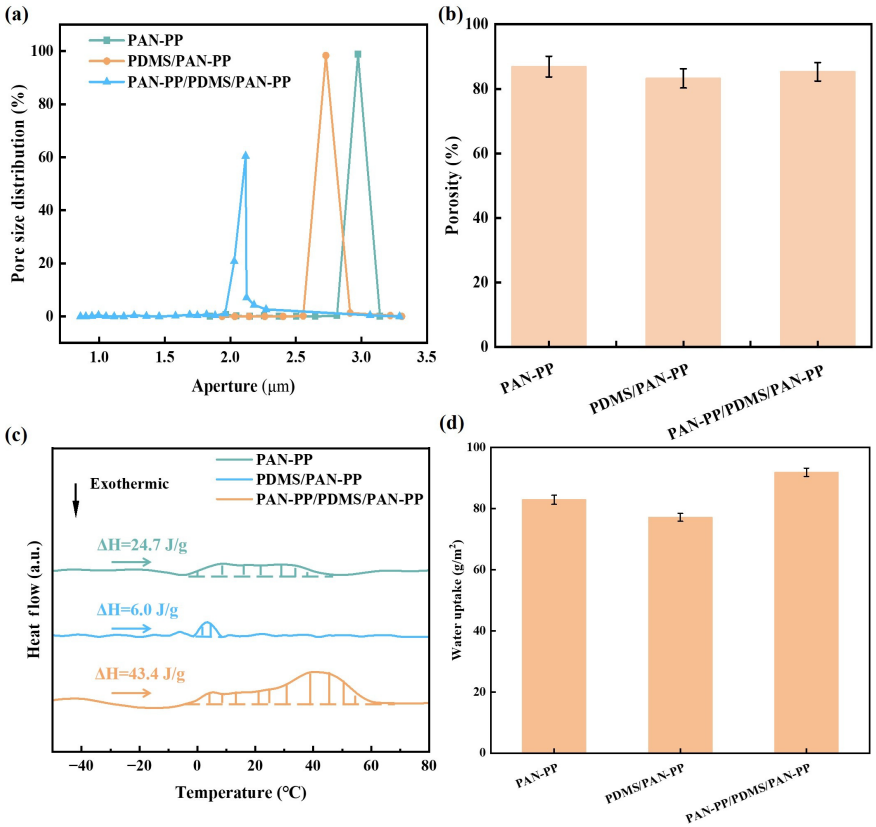

Figure 4. (**a**) The mean effective pore size and (**b**) porosity of PAN-PP, PDMS/PAN-PP and PAN-PP/PDMS/PAN-PP membranes. (**c**) DSC curves of as-prepared membranes showing the presence of water in the membranes. (**d**) Water uptake capability of as-prepared membranes.

3.2. Wetting Property of the as-Prepared Membranes

The wetting performance of the as-prepared membranes were characterized. As shown in Figure 5a, for the PAN-PP membrane, a water droplet with a WCA of about 21.8° in air spread rapidly and permeated through the membrane within 0.3 s. This behavior was attributed to the presence of numerous hydrophilic groups and the formation of a porous structure as aforementioned [31]. The PDMS/PAN-PP membrane exhibited stable super-hydrophobicity with a WCA of 153°, which could be attributed to the hydrophobic PDMS microdomains on its surface. In contrast, the WCA of the PAN-PP/PDMS/PAN-PP membrane decreased from 92.8° to 0° within 9 s, indicating that the coverage with the PAN-PP selective layer significantly improved the hydrophilicity of the PDMS/PAN-PP membrane. The UOCA (n-octane) of PAN-

PP, PDMS/PAN-PP, and PAN-PP/PDMS/PAN-PP tri-layer membranes were 150°, 125° and 165°, respectively. Correspondingly, the underwater chloroform contact angles of the as-prepared membranes were 153°, 128°, 160°, respectively (Figure 5b). The UOCA of PDMS/PAN-PP membrane exhibited obviously decrease, which could be attributed to the oleophilicity of PDMS microdomains facilitating oil spreading. Conversely, the PAN-PP/PDMS/PAN-PP tri-layer configuration demonstrated enhanced underwater oleophobicity, owing to surface roughness and hydrophilic selective layer modulating its wettability (Figure 5c). Notably, the PAN-PP/PDMS/PAN-PP membrane exhibited oil-independent superoleophobicity (UOCA > 150°) and maintained environmental stability across a pH range of 2–12 and various salinity gradients (Figure 5d,e).

To uncover the reasons of the observed wettability, we further analyzed the apparent surface energy of the as-prepared membranes. Figure 5f revealed a 65% reduction in surface energy for PDMS/PAN-PP membranes versus PAN-PP controls, originating from synergistic effects of the intrinsic low surface energy of PDMS and increased roughness as aforementioned [36]. The total surface energy of PAN-PP/PDMS/PAN-PP membrane exhibited 132% higher than that of PDMS/PAN-PP membrane. This structural reorganization-involving PDMS-mediated wettability gradients and roughness modulation-directly correlates with the macroscopic wetting behavior, validating the structure-property correlation [37,38].

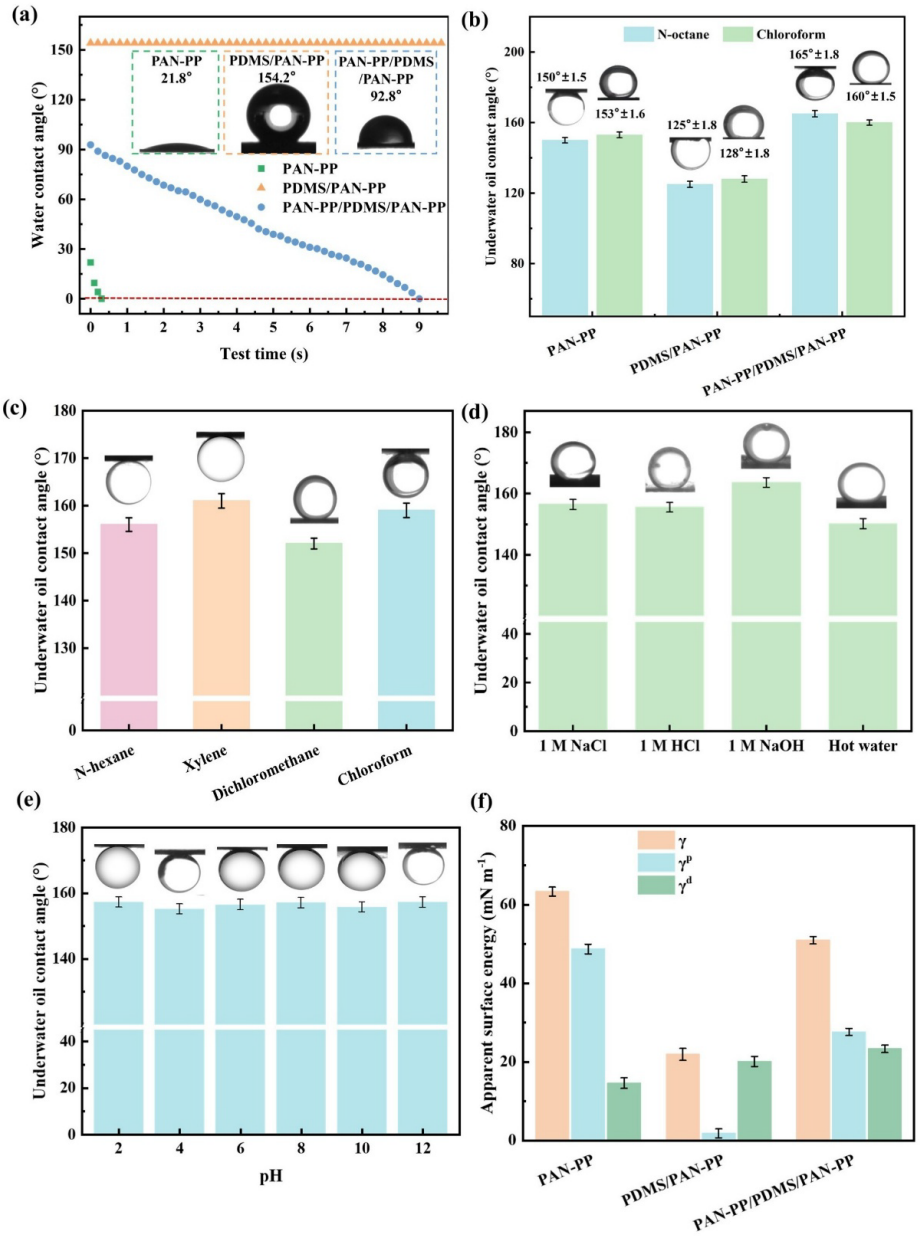

Figure 5. (**a**) WCAs and (**b**) UOCAs of PAN-PP, PDMS/PAN-PP and PAN-PP/PDMS/PAN-PP membranes; (**c**) UOCAs of various oils of PAN-PP/PDMS/PAN-PP membrane; (**d**) UOCAs of the PAN-PP/PDMS/PAN-PP membrane in different water environments (the oil is dichloromethane); (**e**) UOCAs of the PAN-PP/PDMS/PAN-PP membrane in different pH solution (the oil is n-octane); (**f**) Apparent surface energy of PAN-PP, PDMS/PAN-PP and PAN-PP/PDMS/PAN-PP membranes.

 https://doi.org/10.53941/ges.2026.100005

3.3. Performance of Emulsion Separation

The separation performance of as-prepared membranes was investigated in Figure 6a,b. The PAN-PP, PDMS/PAN-PP and PAN-PP/PDMS/PAN-PP membranes exhibited permeance of 13,760 $L \cdot m^{-2} \cdot h^{-1} \cdot bar^{-1}$, 15,497 $L \cdot m^{-2} \cdot h^{-1} \cdot bar^{-1}$ and 22,308 $L \cdot m^{-2} \cdot h^{-1} \cdot bar^{-1}$, respectively, with separation efficiencies of 99.61%, 99.43% and 99.97%, respectively. The wettability gradient of the PDMS/PAN-PP and the PAN-PP/PDMS/PAN-PP nanofiber membranes induced supplementary Laplace forces accelerating water permeation [39]. Meanwhile, the high porosity exceeding 80% might also contribute to the high permeance of the as-prepared membranes. Notably, the TOC content in the filtrate of the PAN-PP, PDMS/PAN-PP and PAN-PP/PDMS/PAN-PP membranes stood at 31 ppm, 46 ppm and 3 ppm, respectively, indicating that the designed hetero-wetting membrane possessed the higher treatment capacity to meet both domestic and international standards (OSPAR:30 ppm, China standards:10 ppm). The treated water not only can be reused in various aspects such as cooling, cleaning, and greening in the factory, significantly saving fresh water resources, but also prevent toxic oily substances from entering natural water bodies to accumulate in aquatic organisms. In addition, digital and optical microscopic images revealed that the n-octane-in-water emulsion appeared turbid before separation, but became clear after filtration through the PAN-PP/PDMS/PAN-PP membrane, with no visible oil droplets observed under microscopy (Figure 6c). The average particle size of oil droplets in the emulsion was measured to be around 488 nm, while the average particle size of oil droplets in the filtrate decreased drastically to below 50 nm (Figure 6d).

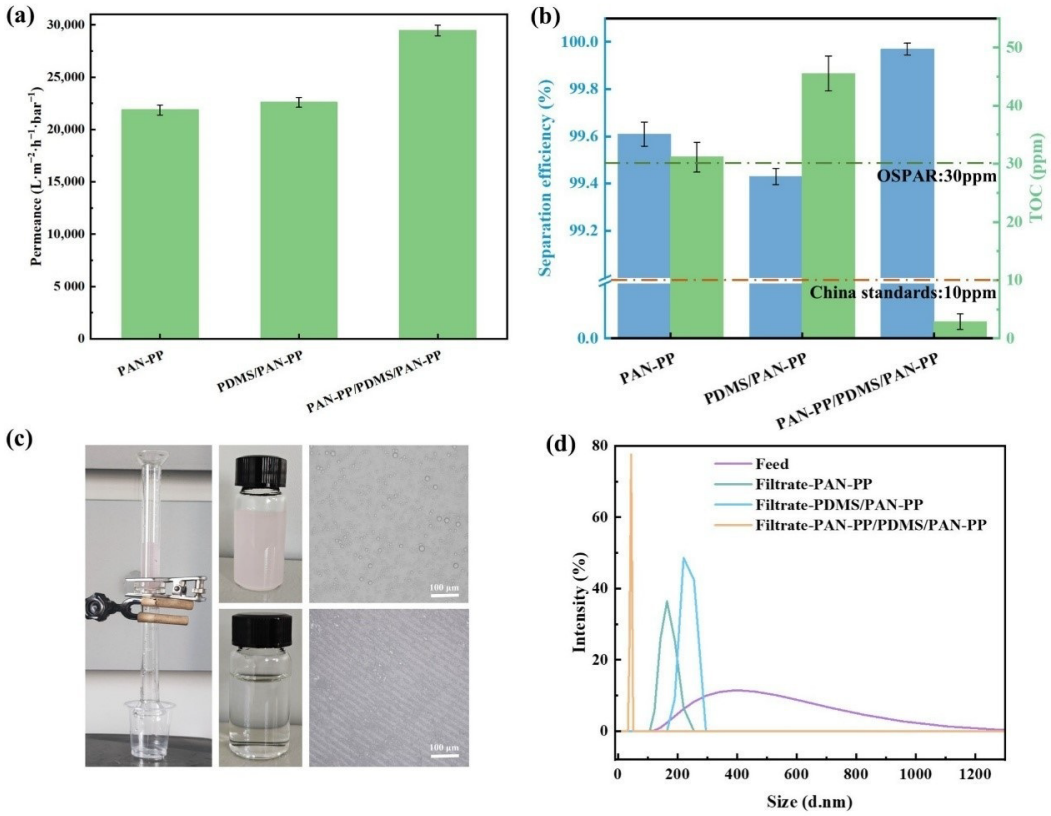

Figure 6. (**a**) Emulsion permeances and (**b**) separation efficiency and TOC content of PAN-PP, PDMS/PAN-PP and PAN-PP/PDMS/PAN-PP membranes; (**c**) Filtration apparatus and optical microscopy images of the emulsion before and after filtration; (**d**) Particle size and distribution of the emulsion before and after filtration.

The cyclic separation experiments were carried out to analyze the anti-fouling performance under the same experimental conditions. After 20 separation cycles, the emulsion permeance of the PAN-PP/PDMS/PAN-PP membrane stabilized within the range of 21,676 to 22,848 $L \cdot m^{-2} \cdot h^{-1} \cdot bar^{-1}$(Figure 7a) with separation above 99.93%, indicating that the hetero-wetting membrane exhibited excellent stability and reusability. No obvious swelling phenomenon was observed for the as-prepared PAN-PP/PDMS/PAN-PP membrane. The IRF and PRR of the PAN-PP/PDMS/PAN-PP membrane reached 4.4% and 94.6%, respectively (Figure 7b), which indicated that the PAN-PP/PDMS/PAN-PP membrane was more durable than the PAN-PP and PDMS/PAN-PP membranes. The reason could be attributed that the PDMS middle layer increased the surface roughness (Ra) from 1.53 μm to 3.32 μm, which can increase the UOCA from 150° to 165° for higher anti-oil-fouling performance.

After 60 min of separation cycles, the PAN-PP/PDMS/PAN-PP membrane maintained low TOC levels and high separation efficiency in cyclic separation (Figure S9a–c). Furthermore, the membrane retained its wettability with WCA of 98° and UOCA of 157° (Figure S9d), confirming the membranes with excellent anti-fouling performance. Furthermore, after a series of stretching and bending process, the UOCA of the PAN-PP/PDMS/PAN-PP nanofiber membrane didn't change significantly and remained stable at approximately 155.2°, achieving underwater superhydrophobicity (UOCA > 150.0°) (Figure 7 c,d). The emulsion separation performance of the PAN-PP/PDMS/PAN-PP membrane outperformed previously reported superhydrophilic nanofiber membranes, as displayed in Table 1 [9,17,31,40–46]. These results collectively demonstrate the structural-engineered membrane's effectiveness in oily emulsion separation through synergistic wettability gradients and surface energy modulation.

Table 1. Comparison of the separation performance of our membrane against that of other superhydrophilic nanofiber membranes reported in the literature.

Membrane	Separation Substances and Efficiency	Permeance ($L \cdot m^{-2} \cdot h^{-1} \cdot bar^{-1}$)	Droplets Size in Filtration	Ref.
PVDF-PG/KH792	Dodecane, soybean > 99.0%	377–7166	/	[9]
H-PLA-AS	N-octane > 99.6%	21,000	68–142 nm	[31]
PAN-PPG-AS	N-octane, toluene	22,206	68–122 nm	[40]
PVDF-PEG-SiO_2	Toluene > 99.57%	6780	~1000 nm	[41]
CS/PVA-SMa	N-octane > 99.5%	21,000	78–280 nm	[42]
LDH@DCA	N-hexane, petroleum ether, soybean > 98.93%	2000–27,346	/	[43]
PAN-COF	N-octane > 99.3%	34,000	~110 nm	[44]
GO@SiO_2	Chloroform, soybean > 99%	654.11	/	[45]
GFM/SSP	Diesel, n-hexane, petroleum ether > 99.8%	2600	/	[46]
PAN-PP/PDMS/-AN-PP	N-octane > 99.97%	22,308	>50 nm	This work

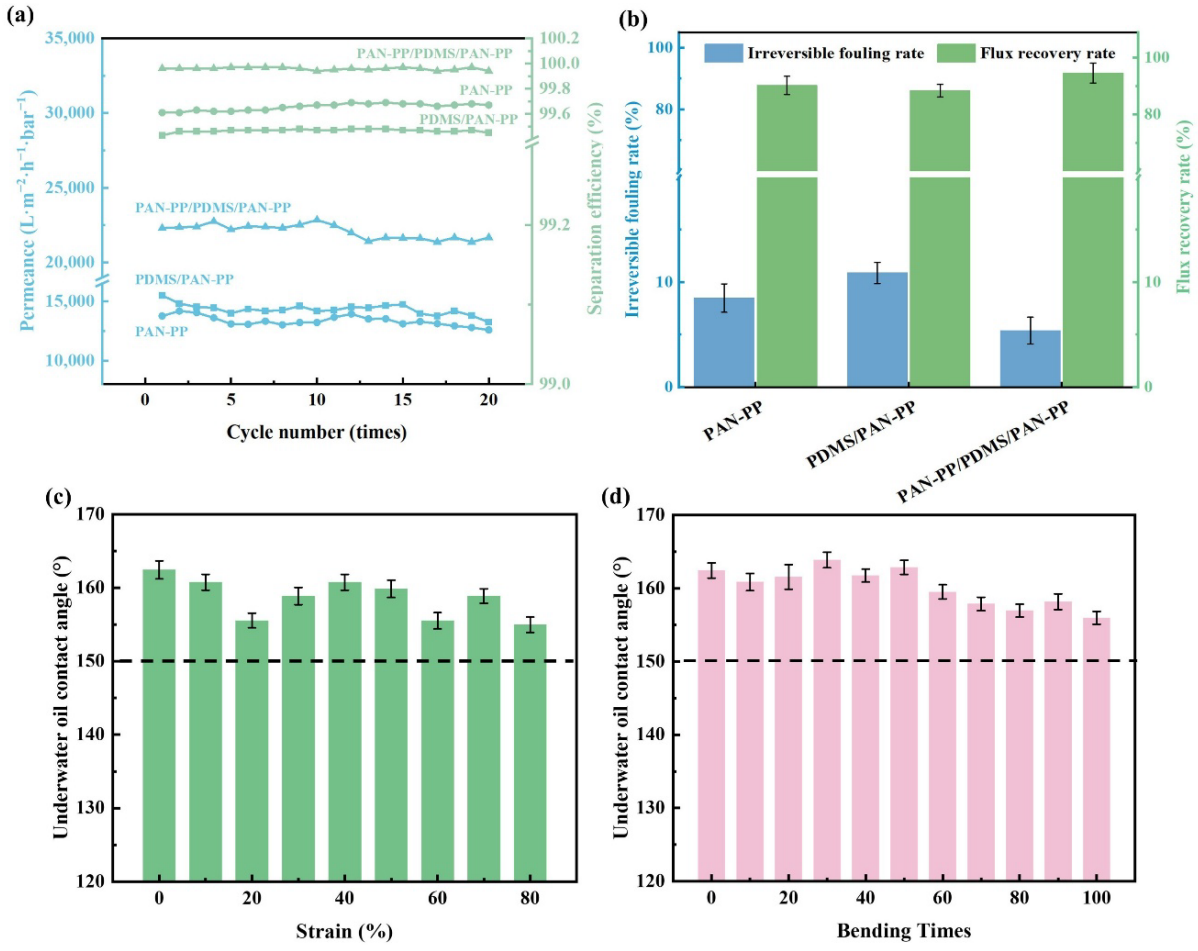

Figure 7. (**a**) Changes in permeance and efficiency with increasing cycle number; (**b**) Irreversible fouling and permeance recovery during separation cycles of the prepared membranes; (**c**) UOCA of the PAN-PP/PDMS/PAN-PP membrane after stretching; (**d**) UOCA of the PAN-PP/PDMS/PAN-PP membrane after curling and bending.

 https://doi.org/10.53941/ges.2026.100005

3.4. Mechanism of the Membrane Separation

The PAN-PP/PDMS/PAN-PP membrane is fabricated by incorporating hydrophobic PDMS microdomains into hydrophilic PAN-PP fibers. The hetero-wetting structure of PAN-PP/PDMS/PAN-PP can be regarded as the composite of hydrophilic selective layer and Janus structure (thin hydrophobic layer and thick hydrophilic layer). To clearly clarify the highly efficient emulsion separation efficiency of the hetero-wetting PAN-PP/PDMS/PAN-PP membrane, we proposed a three-step "sieving-repulsion-adsorption" mechanism as shown in Figure 8. During the "sieving" process, oil droplets larger than the pore size of the nanofiber membrane (2.1 μm) are unable to pass through the PAN-PP/PDMS/PAN-PP membrane. For the "repulsion" process, the PAN-PP hydrophilic selective layer has rich hydrophilic groups and exhibits excellent underwater superoleophobicity. Due to the strong water affinity of selective layer, the membrane surface will form a stable water/solid composite interface. The oil intrusion pressure ΔP can be calculated by the following equation.

$$\Delta P = -\frac{2\gamma_{ow}\cos\theta}{r} \quad (5)$$

where γ_{ow} is the oil/water surface tension. θ is the oil contact angle underwater, and r represents the radius of meniscus. Due to the underwater superoleophobicity of selective layer, $\cos\theta < 0$, therefore $\Delta P > 0$. Meanwhile, for water intrusion pressure, the water contact angle is less than 90°, and $\Delta P < 0$. Thus, the water can penetrate into the pores of the fiber membrane, while oil droplets find it difficult to pass through the PAN-PP selective layer. In the "adsorption" stage, the superhydrophobic PDMS microdomains provide enough adsorption sites for further adsorb tiny oil droplets (sub-150 nm) in the filtrate throughout the emulsion separation process, thereby enhancing separation efficiency. In addition, an imbalanced force (F) at the hydrophobic microdomain boundary acts as the primary driving force for nearby oil droplets. The equation can be calculated as follows [18]:

$$F \approx \gamma_{oil}(\cos\theta_{oleophilic\ surface} - \cos\theta_{oleophobic\ surface}) \quad (6)$$

where γ_{oil} is the surface tension of oil, $\theta_{oleophilic\ surface}$ and $\theta_{oleophobic\ surface}$ are the oil contact angles on the oleophilic PDMS microdomain surface and the oleophobic PAN-PP surface, respectively. In our cases, due to the difference between $\theta_{oleophilic\ surface}$ and $\theta_{oleophobic\ surface}$, a driving force is generated to propel oil droplets towards the oleophilic PDMS microdomains. The Janus structure, composed by PDMS/PAN-PP, could generate the difference in Laplace force under the synergistic effect of superhydrophobic/hydrophilic layers and thereby increasing the emulsion separation permeance [47–50]. As a result, the design of hydrophilic/hydrophobic/hydrophilic structure facilitates water permeation while enhancing the rejection and adsorption of oil droplets. This enables efficient removal of oil droplets with diameter of sub-150 nm from oil-in-water emulsions.

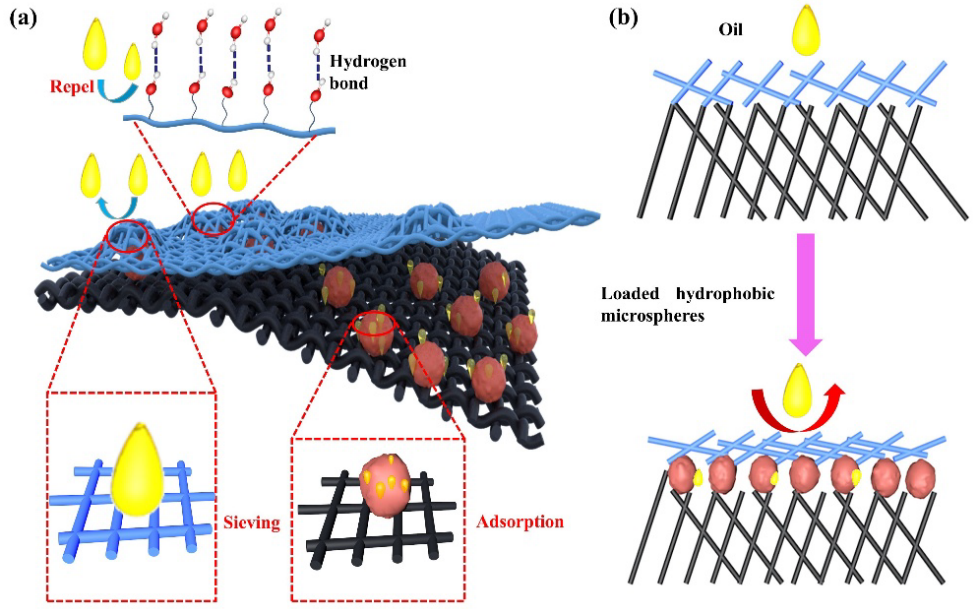

Figure 8. (**a**) Emulsion separation mechanism and (**b**) schematic illustration of oil droplets repulsion of the hetero-wetting PAN-PP/PDMS/PAN-PP membrane.

4. Conclusions

In conclusion, a novel hydrophilic/hydrophobic/hydrophilic hetero-wetting membrane (PAN-PP/PDMS/PAN-PP) was fabricated via an alternative electrospinning-spray method combining hydrophilic modification techniques. The constructed membrane effectively bridges the gap between its large pore sizes and small emulsion droplets due to the combined effect of the

hydrophobic and hydrophilic layers. On the basis of "sieving-repulsion-adsorption" separation mechanism, water can pass smoothly through the PAN-PP/PDMS/PAN-PP membrane, while most large oil droplets are repelled by the hydrophilic PAN-PP selective layer and a small part of smaller oil droplets are further adsorbed by the intercalated PDMS microdomains. As a result, the prepared membranes exhibited outstanding emulsion permeance of 22,308 $L \cdot m^{-2} \cdot h^{-1} \cdot bar^{-1}$, along with a separation efficiency reaching up to 99.97% and TOC content less than 3 ppm, which is superior to most state-of-the-art membranes. Moreover, the hetero-wetting PAN-PP/PDMS/PAN-PP membrane can efficiently remove sub-150 nm oil droplets and demonstrate robust reusability even after 20 cycles of filtration experiments. Compared to the single superwetting PAN-PP membrane lacking a hydrophobic layer, this work achieves highly efficient separation of oil-in-water emulsions, indicating potential applications in stable oil/water emulsion separation, offshore oil spill treatment and oily wastewater resource utilization.

Supplementary Materials

The additional data and information can be downloaded at: https://media.sciltp.com/articles/others/2601081418512374/GES-25100038-Supplementary-Materials.pdf. Figure S1: Emulsion permeance and separation efficiency of PAN-PP/PDMS/PAN-PP membrane. Figure S2: Speculated mechanisms of ring-opening-reaction induced PEA/PEGDGE hybridization to realize *in-situ* hydrophilization in PAN-based membranes. Figure S3: (a) Schematic illustration of the PDMS/PAN-PP membrane. SEM images of the PDMS/PAN-PP membrane fabricated at different PDMS concentration conditions of (b) 2%; (c) 5%, (d) 8%; (e) 10%; (f) 13%. Figure S4: (a) Schematic illustration of the PAN-PP/PDMS/PAN-PP membrane. SEM images of the PAN-PP/PDMS/PAN-PP membrane fabricated at different PDMS concentration conditions of (b) 2%; (c) 5%; (d) 8%; (e) 10%; (f) 13%. Figure S5: Cross-sectional SEM image of the PDMS/PAN-PP membrane. Figure S6: (a) Cross-sectional SEM image of the PAN-PP/PDMS/PAN-PP membrane; (b) SEM image of the selective layer on the PAN-PP fiber. Figure S7: Elemental mapping images of (a) PAN-PP and (b) PAN-PP/PDMS/PAN-PP membranes. Figure S8: Two-dimensional Raman surface scanning of (a) PDMS/PAN-PP and (b,c) PAN-PP/PDMS/PAN-PP membranes. Figure S9: Long separation cycle performance of (a) PAN-PP; (b) PDMS/PAN-PP and (c) PAN-PP/PDMS/PAN-PP membranes; (d) The WCA and UOCA of the PAN-PP/PDMS/PAN-PP membrane before and after 20 separation cycles.

Author Contributions

L.Y.: Funding acquisition, Project administration, Writing—original draft; M.Z.: Investigation, Data curation, Formal analysis; C.C.: Data curation, Formal analysis; M.Z.: Supervision; K.W.: Conceptualization; Y.G.: Data curation, Supervision; P.L.: Methodology; D.L.: Data curation, Visualization; X.C.: Formal analysis, Writing—review and editing, Funding acquisition. All authors have read and agreed to the published version of the manuscript.

Funding

This work was supported by National Natural Science Foundation of China (22406042, 52573109), Natural Science Foundation of Shandong Province (ZR2024ME231, ZR2024QE258), State Key Laboratory of Urban-rural Water Resources and Environment(Harbin Institute of Technology) (No.2025TS37), Science and Technology Project of the Hebei Academy of Sciences (25702), Fundamental Research Funds for the Central Universities (HIT.OCEF.2024031) and Guangxi First-class Disciplines (Agricultural Resources and Environment).

Institutional Review Board Statement

Not applicable.

Informed Consent Statement

Not applicable.

Data Availability Statement

Relevant data are available upon request.

Conflicts of Interest

The authors declare no conflict of interest, and there is no specific financial interest related to Shandong Sino-European Membrane Technology Research Institute Co., Ltd.

Use of AI and AI-assisted Technologies

No AI tools were utilized for this paper.

References

1. Wang, Z.; Guo, P.; Heng, L.; et al. Nano/Submicrometer-Emulsion Oily Wastewater Treatment Inspired by Plant Transpiration. *Matter* **2021**, *4*, 1274–1286.
2. He, L.; Qi, X.; Wei, W.; et al. Biomass-Activated Carbon-Based Superhydrophobic Sponge with Photothermal Properties for Adsorptive Separation of Waste Oil. *J. Hazard. Mater.* **2024**, *477*, 135222.
3. Cui, W.; Fan, T.; Li, Y.; et al. Robust Functional Janus Nanofibrous Membranes for Efficient Harsh Environmental Air Filtration and Oil/Water Separation. *J. Membr. Sci.* **2022**, *663*, 121018.
4. Tong, Y.; Qi, M.; Sun, P.; et al. Estimation of Unintended Treated Wastewater Contributions to Streams in the Yangtze River Basin and the Potential Human Health and Ecological Risk Analysis. *Environ. Sci. Technol.* **2022**, *56*, 5590–5601.
5. Tanudjaja, H.J.; Hejase, C.A.; Tarabara, V.V.; et al. Membrane-Based Separation for Oily Wastewater: A Practical Perspective. *Water Res.* **2019**, *156*, 347–365.

6. Peterson, C.H.; Rice, S.D.; Short, J.W.; et al. Long-Term Ecosystem Response to the Exxon Valdez Oil Spill. *Science* **2003**, *302*, 2082–2086.
7. Wang, Y.; Villalobos, L.F.; Liang, L.; et al. Scalable Weaving of Resilient Membranes with On-Demand Superwettability for High-Performance Nanoemulsion Separations. *Sci. Adv.* 2024, *10*, eadn3289.
8. Wu, S.; Lu, F.; Deng, R.; et al. Solar-Driven Evaporators with Thin-Film-Composite Architecture Inspired by Plant Roots for Treating Concentrated Nano-/Submicrometer Emulsions. *ACS Appl. Mater. Interfaces* **2022**, *14*, 51555–51563.
9. Chen, J.; Zhang, Z.; Han, J.; et al. A Simple One-Step Method to Synthesize PVDF-PG/KH792 Membrane for Separation of Oil-in-Water Emulsions. *J. Water Process Eng.* **2021**, *41*, 101996.
10. Lin, Y.; Yu, F.; Yu, Z.; et al. Mussel-Inspired Superhydrophilic and Antibacterial Membranes for Effective Gravity-Driven Separation of Oil-in-Water Emulsions. *Sep. Purif. Technol.* **2024**, *341*, 126919.
11. Wang, B.; Luo, X.; Feng, Y.; et al. Turbo-Synergistic Oily Wastewater Remediation in Bio-Inspired Cone Array Barrel. *Adv. Sci.* **2022**, *9*, 2204244.
12. Chen, D.; Bao, M.; Ge, H.; et al. A Hydrogel-Coated Wood Membrane with Intelligent Oil Pollution Detection for Emulsion Separation. *Small* **2024**, *20*, 2401719.
13. Zhang, J.; Peng, K.; Xu, Z.-K.; et al. A Comprehensive Review on the Behavior and Evolution of Oil Droplets during Oil/Water Separation by Membranes. *Adv. Colloid Interface Sci.* **2023**, *319*, 102971.
14. Ge, J.; Zong, D.; Jin, Q.; et al. Biomimetic and Superwettable Nanofibrous Skins for Highly Efficient Separation of Oil-in-Water Emulsions. *Adv. Funct. Mater.* **2018**, *28*, 1705051.
15. Guo, X.; Zhao, L.; Li, H.; et al. Janus Channel of Membranes Enables Concurrent Oil and Water Recovery from Emulsions. *Science* **2024**, *386*, 654–659.
16. Meng, Z.; Zhu, L.; Wang, X.; et al. Electrospun Nanofibrous Composite Membranes for Separations. *Acc. Mater. Res.* **2023**, *4*, 180–192.
17. Cheng, X.; Li, T.; Yan, L.; et al. Biodegradable Electrospinning Superhydrophilic Nanofiber Membranes for Ultrafast Oil-Water Separation. *Sci. Adv.* **2023**, *9*, eadh8195.
18. Zhang, X.; Zhu, Y.; Zhang, F.; et al. Hydrophilic/Hydrophobic Nanofibres Intercalated Multilayer Membrane with Hierarchical Structure for Efficient Oil/Water Separation. *Sep. Purif. Technol.* **2022**, *288*, 120672.
19. Ge, J.; Ye, Y.; Yao, H.; et al. Pumping through Porous Hydrophobic/Oleophilic Materials: An Alternative Technology for Oil Spill Remediation. *Angew. Chem.* **2014**, *126*, 3686–3690.
20. Yang, J.; Li, H.; Chen, Z.; et al. Janus Membranes with Controllable Asymmetric Configurations for Highly Efficient Separation of Oil-in-Water Emulsions. *J. Mater. Chem. A* **2019**, *7*, 7907–7917.
21. Hu, Y.; Li, H.; Xu, Z. Janus Hollow Fiber Membranes with Functionalized Outer Surfaces for Continuous Demulsification and Separation of Oil-in-Water Emulsions. *J. Membr. Sci.* **2022**, *648*, 120388.
22. Li, X.; Zhang, W.; Qu, R.; et al. Asymmetric Superwetting Configuration of Janus Membranes Based on Thiol-Ene Clickable Silane Nanospheres Enabling On-Demand and Energy-Efficient Oil-Water Remediation. *J. Mater. Chem. A* **2019**, *7*, 10047–10057.
23. Zhang, M.; Yang, Q.; Gao, M.; et al. Fabrication of Janus Cellulose Nanocomposite Membrane for Various Water/Oil Separation and Selective One-Way Transmission. *J. Environ. Chem. Eng.* **2021**, *9*, 106016.
24. Qin, Y.; Shen, H.; Han, L.; et al. Mechanically Robust Janus Poly (Lactic Acid) Hybrid Fibrous Membranes toward Highly Efficient Switchable Separation of Surfactant-Stabilized Oil/Water Emulsions. *ACS Appl. Mater. Interfaces* **2020**, *12*, 50879–50888.
25. Huang, X.; Wu, Z.; Zhang, S.; et al. Mechanically Robust Janus Nanofibrous Membrane with Asymmetric Wettability for High Efficiency Emulsion Separation. *J. Hazard. Mater.* **2022**, *429*, 128250.
26. Zeng, X.; Qian, L.; Yuan, X.; et al. Inspired by Stenocara Beetles: From Water Collection to High-Efficiency Water-in-Oil Emulsion Separation. *ACS Nano* **2017**, *11*, 760–769.
27. Jiang, X.; Yang, F.; Xu, G.; et al. Smart NiAl-LHDs-Based Superwetting Janus Membrane Based on Charge Demulsification for Efficient Separation of Multiple Emulsions and Mixtures via Multi-Strategy Synergy. *Sep. Purif. Technol.* **2023**, *323*, 124350.
28. Du, L.; Quan, X.; Fan, X.; et al. Electro-Responsive Carbon Membranes with Reversible Superhydrophobicity/Superhydrophilicity Switch for Efficient Oil/Water Separation. *Sep. Purif. Technol.* **2019**, *210*, 891–899.
29. Wei, X.; Naraginti, S.; Yang, X.; et al. Polydopamine Functionalized $FeVO_4$@PVDF Ultrafiltration Membrane with Superior Antifouling and Detoxification Properties. *Chem. Eng. J.* **2024**, *497*, 154718.
30. Zou, D.; Nie, D.; Wang, W.; et al. Fabrication of a MoS_2@PAN Composite Membrane for Efficient Removal of Toxic Cr (VI). *Desalination* **2025**, *600*, 118460.
31. Cheng, X.; Sun, Z.; Yang, X.; et al. Construction of Superhydrophilic Hierarchical Polyacrylonitrile Nanofiber Membranes by *in Situ* Asymmetry Engineering for Unprecedently Ultrafast Oil-Water Emulsion Separation. *J. Mater. Chem. A* **2020**, *8*, 16933–16942.
32. Cheng, X.; Jiao, Y.; Sun, Z.; et al. Constructing Scalable Superhydrophobic Membranes for Ultrafast Water-Oil Separation. *ACS Nano* **2021**, *15*, 3500–3508.
33. Zhou, H.; Su, Y.; Chen, X.; et al. Plasma Modification of Substrate with Poly(Methylhydrosiloxane) for Enhancing the Interfacial Stability of PDMS/PAN Composite Membrane. *J. Membr. Sci.* **2016**, *520*, 779–789.
34. Li, X.; Zhang, L.; Yang, Z.; et al. Hydrophobic Modified Activated Carbon Using PDMS for the Adsorption of VOCs in Humid Condition. *Sep. Purif. Technol.* **2020**, *239*, 116517.
35. Wang, Y.; Yu, Z.; Dufresne, A.; et al. Quantitative Analysis of Compatibility and Dispersibility in Nanocellulose-

Reinforced Composites: Hansen Solubility and Raman Mapping. *ACS Nano* **2021**, *12*, 20148–20163.
36. Liu, Y.; Wang, X.; Feng, S. Nonflammable and Magnetic Sponge Decorated with Polydimethylsiloxane Brush for Multitasking and Highly Efficient Oil–Water Separation. *Adv. Funct. Mater.* **2019**, *29*, 1902488.
37. Shen, Q.; Jiang, Y.; Guo, S.; et al. One-Step Electrospinning Membranes with Gradual-Transition Wettability Gradient for Directional Fluid Transport. *J. Membr. Sci.* **2022**, *644*, 120091.
38. Yang, X.; Wen, Y.; Li, Y.; et al. Engineering *in Situ* Catalytic Cleaning Membrane via Prebiotic-Chemistry-Inspired Mineralization. *Adv. Mater.* **2023**, *35*, 2306626.
39. Zhuang, Z.; Wu, K.; Zhang, T.; et al. One-Step Fabrication of Robust Stenocara Beetle-Inspired Membrane Deriving from Polyethylene Terephthalate (PET) Waste for Enhancing Emulsion Separation. *Sep. Purif. Technol.* **2024**, *351*, 128128.
40. Ge, J.; Jin, Q.; Zong, D.; et al. Biomimetic Multilayer Nanofibrous Membranes with Elaborated Superwettability for Effective Purification of Emulsified Oily Wastewater. *ACS Appl. Mater. Interfaces* **2018**, *10*, 16183–16192.
41. Zhong, X.; Shi, Q.; Guo, Z. Synergistic Construction of Superhydrophilic PVDF Membranes by Dual Modification Strategies for Efficient Emulsion Separation. *Small* **2024**, *20*, e2402538.
42. Cheng, X.; Zhang, J.; Yan, L.; et al. Biodegradable Nanofiber Membranes Based on Interpenetrating Network for Highly Efficient Oil/Water Separation. *Adv. Compos. Hybrid Mater.* **2024**, *7*, 197.
43. Ning, D.; Lu, Z.; Tian, C.; et al. Hierarchical and Superwettable Cellulose Acetate Nanofibrous Membranes Decorated via 3D Flower-Like Layered Double Hydroxides for Efficient Oil/Water Separation. *Sep. Purif. Technol.* **2024**, *342*, 127052.
44. Zhou, M.; Zhou, J.; Yan, L.; et al. Engineering Superhydrophilic and Fouling-Free COF Armor for Ultrafast Oil–Water Separation. *Small* **2025**, *21*, 2505330.
45. Feng, L.; Gao, Y.; Xu, Y.; et al. A Dual-Functional Layer Modified GO@SiO_2 Membrane with Excellent Anti-Fouling Performance for Continuous Separation of Oil-in-Water Emulsion. *J. Hazard. Mater.* **2021**, *420*, 126681.
46. Xu, L.; Xu, T.; Liu, W.; et al. Heterogeneous Wettability Membrane for Efficient Demulsification and Separation of Oil-in-Water Emulsions. *Chem. Eng. J.* **2024**, *489*, 151466.
47. Li, X.; Gui, Q.; Wei, Y.; et al. Novel Superwetting Nanofibrous Skins for Removing Stubborn Soluble Oil in Emulsified Wastewater. *J. Mater. Chem. A* **2021**, *9*, 26127–26134.
48. Zhou, M.; Tong, J.; Zhou, F.; et al. Constructing Heterogeneously Wettable Nanofiber Membrane for Highly Efficient Oil Refining. *Adv. Membr.* **2025**, *5*, 100135.
49. Wu, J.; Wang, N.; Wang, L.; et al. Unidirectional Water-Penetration Composite Fibrous Film via Electrospinning. *Soft Matter* **2012**, *8*, 5996–5999.
50. Yang, H.; Hou, J.; Chen, V.; et al. Janus Membranes: Exploring Duality for Advanced Separation. *Angew. Chem. Int. Ed.* **2016**, *55*, 13398–13407.